JSEE Vol. 22, No. 3, 2020 DOI:10.48303/jsee.2020.246981

Research Paper

Seismic Fragility of Low-Rise RC Frames with Construction Deficiencies Subjected to Mainshock-Aftershock Sequences

Siavash Sadeghi[1], Afshin Kalantari[2], and Esmaeel Izadi Zaman Abadi[3]*

1. Ph.D. Candidate, Department of Civil Engineering, Najafabad Branch, Islamic Azad University, Najafabad, Iran
2. Associate Professor, Structural Engineering Research Center, International Institute of Earthquake Engineering and Seismology (IIEES), Tehran, Iran
3. Assistant Professor, Department of Civil Engineering, Najafabad Branch, Islamic Azad University, Najafabad, Iran, *Corresponding Author; email: e.izadi@pci.iaun.ac.ir

Received: 11/01/2021
Revised: 04/09/2021
Accepted: 10/11/2021

ABSTRACT

The accuracy of local contractors in constructing Low-rise RC structures located in small towns is subjected to substantial fluctuations that increase the vulnerability of these structures, especially when sequential excitations are under consideration. Four major construction deficiencies are identified in this study by an initial field survey and are then considered in numerical modeling of a 3-story RC moment frame. The median collapse capacity (MCC) of Low-rise RC moment frames under sequential excitations is evaluated in presence of construction faults identified in a field study. Various mainshock levels represented by their maximum inter-story drifts are then imposed on the as-designed and the deficient structures. Following each mainshock, the median collapse capacities (MCCs) of the structures under the aftershock are computed using the IDA method. Investigating the obtained MCCs showed that unintended increase of the beams' width can help in reducing structure's vulnerability against sequential excitations. Despite this, the comparison of the residual drifts imposed by the mainshocks showed the decreased ductility caused by this construction deficiency. Ranking the MCC reductions caused by the other deficient models, the highest vulnerabilities were posed by the models that caused larger column plasticities at the collapse state and prevented effective yielding of the beams.

Keywords:
Collapse fragility curves; Mainshock-aftershock effects; Low-rise RC frames; Construction deficiency; Modeling method evaluation

1. Introduction

Several study programs are conducted each year with the aim of identifying criteria that can fulfill the safety and economy of structural design methods. Having put all these efforts into practice, a design solution becomes ready and waits to be implemented by the construction process that manufactures the building. The success of the construction process to accurately implement what is specified in the design documents is the final necessary chain that determines the success of the whole process. Field investigations made of constructed buildings reveal that the construction accuracy is dramatically affected by the level of knowledge, awareness and proficiency of the human resources. Lack of these requirements or the low quality of facilities and the hardware may, therefore, lead to construction deficiencies. Controlling and eliminating these faults in practice is a construction management subject. Nonetheless, the effect of these faults on the structural performance of a constructed building is worth studying. Such a study is expected to illuminate important questions including:

a) How sensitive are the structural performance measures to the construction errors?
b) What points should be focused on during a rehabilitation program, regarding the existing deficiencies, so that the program effects are maximized?
c) How the construction deficiencies, increase the vulnerability of the structures built in an urban area? This can be regarded for organizing after-event rescue activities.

According to the importance and applicability of this topic, it has been addressed by a number of previous researches. The first class of studies is devoted to comprehensive surveys that identify and categorize failure causes. These studies do not address the effect of construction failures on performance of the structure. Examples include the studies described in [1] and [2] who carried out surveys on steel bridges and timber structures respectively. Despite these studies that are based on field surveys, computational methods have been employed by the following investigations to evaluate the structural consequences of construction failures. Many studies (e.g. [3-5]) have investigated the effect of random uncontrollable errors on the reliability of a design process. Still, there are other studies that have evaluated consequences of construction deficits on various aspects of structural performance, among which, some address early failure of the structure within the construction phase. As an example, Zhang et al. [6] studied the effect of faults in steel scaffold shoring on the failure of concrete formworks during installation. In another study, El-Shahhat et al. [7] used a scenario-based analysis to investigate the probability of structural failure during construction of reinforce concrete (RC) multi-story buildings. They considered concrete cover, steel yield stress, concrete strength, reinforcement area, and construction cycle as discrete error parameters. Uncertainties involving the rate and magnitude of error parameters as well as the simultaneous occurrence of multiple errors were not addressed in their sensitivity analyses. Later, Epaarachchi et al. [8] and Epaarachchi and Stewart [9] investigated the same problem in the absence and the presence of human errors, respectively. They extended the work of El-Shahhat et al. [7] by considering more parameters and replacing the sensitivity-based assessment with an event-based Monte-Carlo simulation.

Only a few studies have been focused on the performance of structures suffering from construction deficiencies. Hong & He [10] studied the effect of human errors on the reliability of roof structures subjected to wind load. The study by Gashti et al. [11] used an analytical method to evaluate the effects of construction mistakes on amplification of seismic base shear and displacements. As this review indicates, very rare research programs have dealt with the effect of construction and human errors on the risk of collapse of structures during earthquakes.

To address the effect of the multiple excitations of a structure due to a sequence of ground motions, the recent researches treat the earthquake as a sequence of mainshock-aftershock events. The structural damage caused by a mainshock makes the building more prone to collapse under the following aftershocks. Recent studies on this topic (e.g. [12-14]) have revealed the significance of aftershocks in predicting the seismic collapse capacity of structures. Presence of construction flaws will heighten the damage levels expected to threaten a structure subjected to a mainshock. Thus, the damaging effects caused by aftershocks are also expected to intensify for structures with construction faults. Therefore, a complete and accurate evaluation of the effects caused by construction errors will require consideration of mainshock-aftershock sequences. This subject is investigated in the present article.

The aim of this article is to evaluate the effect of construction errors in the range of low-rise RC moment frames by considering mainshock-aftershock effects. For this purpose, a 3-story structure is selected to represent the common urban building type impacted by the 2017 Sarpol-e Zahab earthquake, Iran. The study starts by a field investigation that inspects a number of structures suffering from varying damage levels during the earthquake. Afterwards, a number of more frequent construction faults are identified and their effect on the collapse performance of the selected RC frame is studied. For this purpose, numerical structural models are developed that account for construction errors and are subjected to mainshock-aftershock seismic

analyses. The probabilistic collapse capacities of deficient as-built models are then extracted and compared against as-designed models. The study accounts for the probabilistic nature of earthquake events by considering the variability of ground motions' frequency content. For this purpose, Incremental Dynamic Analysis (IDA) is applied and the collapse capacities of the models are probabilistically expressed using collapse fragility curves. More details about the employed methodology are provided in the next sections.

2. Construction Faults Identification

The first part of the research is a field study to identify the construction faults that are common according to local practicing methods for the construction of RC structures. To identify the deficiencies in built operational structures, non-destructive methods should be used to avoid interruption of the functionality. However, such tests commonly lack the accuracy required for an in-depth investigation. An alternative method is to investigate the buildings that are under construction and to measure as-built characteristics of these buildings. Nevertheless, convincing construction contractors to accommodate with the program is a preventing challenge. Furthermore, the presence of an inspector is likely to reduce the construction deficiencies and may lead to a statistical bias and inaccurate identification of the common errors.

A method that does not suffer from these limitations becomes available after damaging events such as intense earthquakes. Construction details of many damaged structures become exposed in such conditions and make visual inspection and field investigation comfortable and costless. In addition, the damaged structures being inspected are more likely to suffer construction faults and the error identification study will have a higher rate of success. Accordingly, this study makes a field investigation of the buildings suffering damage during the 2017 Sarpol-e Zahab earthquake, Kermanshah, Iran. Regarding the findings of this field study, four main categories of construction deficiencies are identified for RC structures. These deficiencies and an initial discussion on their damaging effects are presented in the following.

2.1. Reinforcement Cover

The concrete cover, in addition to protection of the reinforcement bars against the environmental aggressive conditions, provides lateral bracing to longitudinal reinforcement in areas between the stirrups and impedes buckling of the compressive bars. This role of the cover commonly becomes important only when the stirrups spacing is larger than values suggested by design codes.

While the mentioned functions require the cover thickness to surpass minimum allowable values, a more serious concern stimulates when the cover exceeds the design values. This may happen due to the misalignment of the longitudinal bars or movement of formworks during the casting of the concrete. In this condition, the distribution of loads considered in the design of the section may considerably change. It is worthy to note that previous studies [7-9] also consider the effect of cover thickness following its effect on the *Mn* factor.

The field study on the RC structures damaged by the Sarpol-e Zahab earthquake reveals cover increase values in a 1-5 cm range. Accordingly, this increase reaches around 100% in some cases with respect to the code-specified cover of 50 mm measured from the center of longitudinal bars. The photographs shown in Figure (1) illustrate an example of the structures with this construction

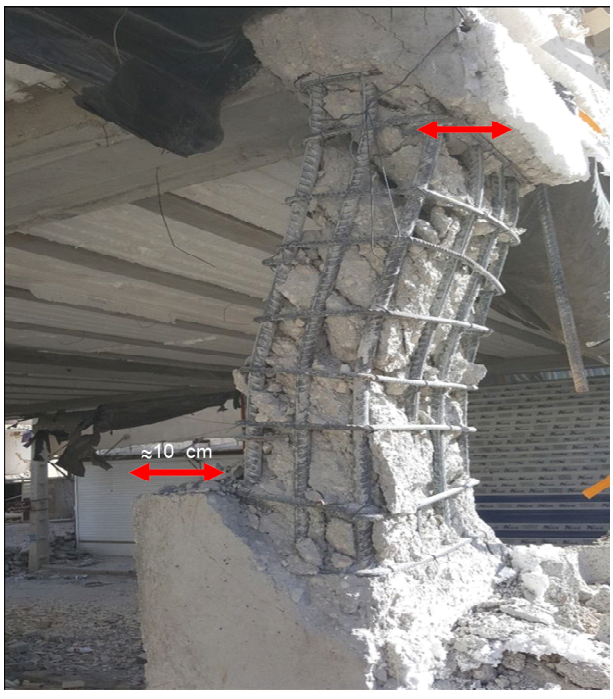

Figure 1. The overly sized concrete cover in columns of a collapsed building in Sarpol-e Zahab 2017 earthquake.

deficiency. To evaluate the worst effect caused by the cover increase deficiency, the performed nu-merical analyses deploy a 100 mm value instead of the as-designed 50 mm value described above.

2.2. Concrete Strength

Another parameter that has a determining effect on the bending capacity of RC members is the compressive strength of the cast-in-place concrete. In urban areas with low population and small-size residential buildings, concrete is commonly produced in-situ using small mixer machines. Thus, the quality of concrete becomes dependent to the skill of workmen, the awareness and accuracy of the inspecting agencies and the quality of available material. Concrete quality, on the other hand, directly affects its compressive strength, $f_c^{'}$.

Again, the field survey and the destructive and non-destructive test results reveal that many of the cast-in-situ concrete used in small-scale residential buildings have values lower than the design values. For example, a report published by IIEES [15] about the Sarpol-e Zahab earthquake, after conducting 100 days of expertise and completing 700 field visit forms, shows that the compressive strength of most concrete buildings is of moderate importance, which must be at least 20 MPa, for various reasons much lower than this value. It should be noted that the strength mentioned in the report is the compressive strength of concrete in a state without earthquake damage. The minor variation in beams' concrete is attributed to the accurate mixing and pouring procedure used in practice for the large-volume concrete of the floor slab and the beams. The employed practical procedure for these parts of the structure used factory-mixed concrete pumped by truck mixers. Therefore, according to this report and field visit, it is possible to reduce the compressive strength of concrete columns between 10% and 40%. To evaluate the worst effect caused by deficiencies in columns' compressive strength on the collapse performance of the studied structure, the 21 N/mm^2 design strength of these members is reduced to 12 N/mm^2 in a deficient version of the as-designed model.

2.3. Height of the first Story

The third parameter identified through the field study as a common construction error is the height of the first story. According to Figure (2), this problem was observed in buildings without a basement where a faulty practice was used for elevating the base level in order to prevent the flow of rain water. The accepted practice for this purpose is to upraise the ground level using stone pitching and then install the footing (or strip) foundation on which the columns are constructed. The faulty method, however, did not elevate the foundation level and used taller columns in order to allow filling of the floor with stone pitching. This deficient method was observed to be a common construction practice in the region. The columns at the first story were thus constructed in an added length approximately equal to 0.8 m. To account for the constraint provided by the rigidity of the infill wall at the base of the column, about 40% of this length was judgmentally considered as the added deformable length. This added length was reflected in the numerical model to evaluate the effect of the lowered flexural strength and stiffness of these columns. Since the special shear reinforcement details provided by the design documents are implemented at the actual bottom of the column, the modeled column base (which is 0.3 m higher than the actual base) does not use these details. This issue affects the ductility capacity of the first story columns by reducing the buckling strength of the flexural reinforcements.

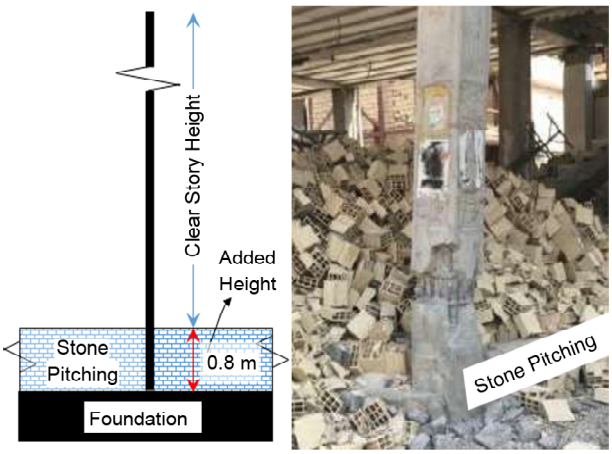

Figure 2. Example of column elongation used instead if foundation elevation to upgrade the building floor.

2.4. Beam Dimensions

In RC construction, the beam and column formworks are commonly dimensioned to achieve the design drawings within acceptable tolerances.

However, some construction conditions may increase the actual cross section obtained for the beams. During the field study, a common cause for this inaccuracy was identified as the joining of cast-in-place RC deck joists to the adjacent RC beams. Detail of the common construction method used in the region by employment of stay-in-place formworks is shown in Figure (3). While enlarging the cross section improves the strength and stiffness of the beams, it may cause detrimental effects on the inelastic collapse mode of the structure by violating the strong-column weak-beam (SCWB) principle. The extent of this violation depends on the level of over-strength provided in the design process for the column sections. A column designed to tightly meet the SCWB principle will experience considerable hinging by the increase of beam capacity. The structures with remarkable column capacity margin with respect to the SCWB principle, on the other hand, will benefit from the beam capacity elevation while the plastic hinge formation in the columns is still prevented. Thus, the effect of the unintended increase in the beams width depends on the design conditions. In Figure (3), a schema of the standard beam section and the beam section generated by aggregating the adjacent joists is also compared.

3. Design and Modeling of a Benchmark Structure

As mentioned in section 1, the sensitivity of seismic collapse capacity of a 3-story RC moment frame to the foregoing construction faults is assessed. As a benchmark structure, the building configuration shown in Figure (4) is adopted, which is a typical configuration frequently used in the Sarpol-e Zahab urban area. Seismic loading of the building is determined following the 4th edition of Iranian National Standard No. 2800 (STD-2800) [16] and the structure is designed following ACI 318-14 specifications [17]. For computing the design base shear, seismic importance factor $I = 1$ has been used along with a design spectral acceleration $A = 0.3g$. In addition, site soil amplification factor $B = 2.5$ has been utilized following soil shear wave velocity

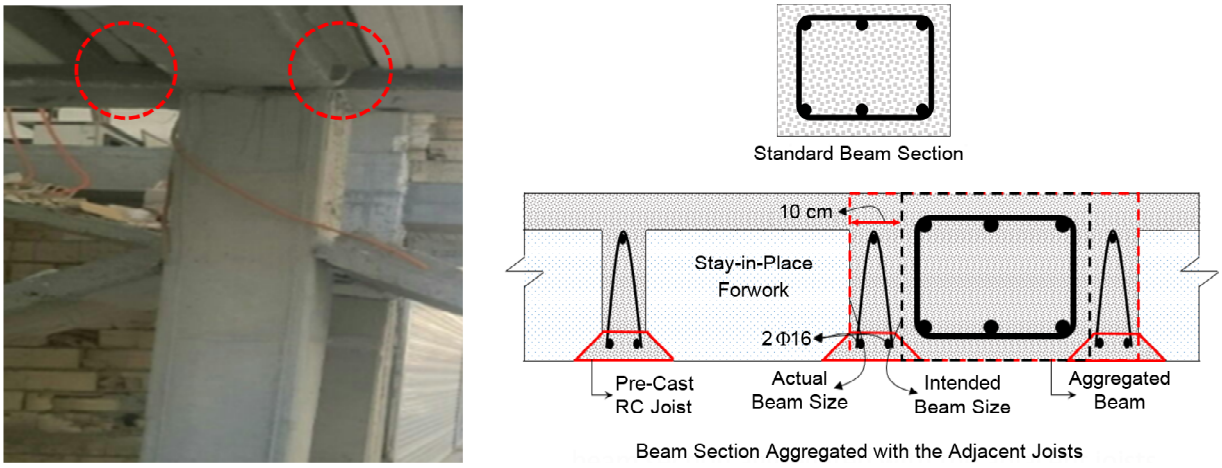

Figure 3. Faulty joining of deck joist to the RC beams and the resulting T-shaped cross section.

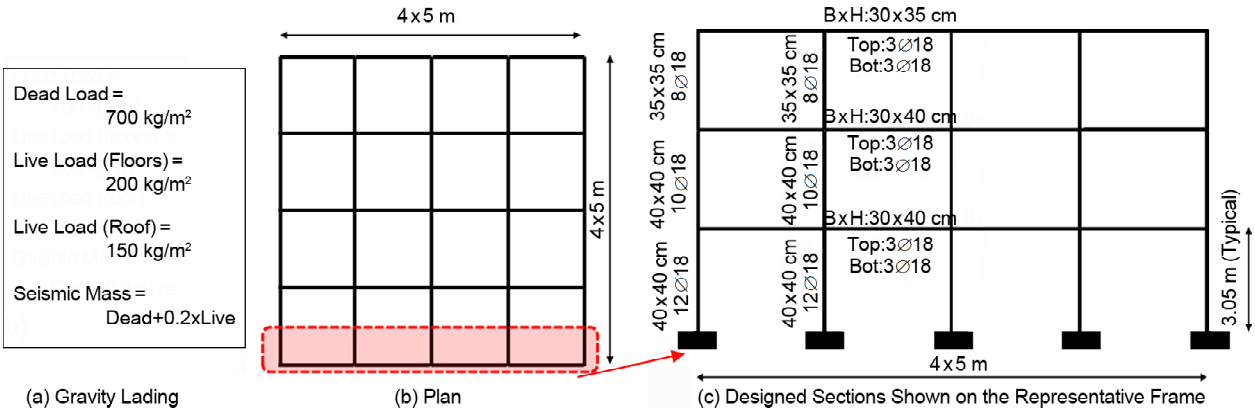

Figure 4. Benchmark building configuration.

reports. Assuming an "intermediate" ductility for the RC moment frame, a response modification factor $R = 5$ was also considered following STD-2800. Using these factors and a fundamental period of $T = 0.382$ sec, a design base shear coefficient $C = 0.15$ was calculated following $C = A \times B \times I/R$ equation of the STD-2800 [16]. The gravitational loading values and the designed RC sections are presented in Figure (4).

To evaluate the effects of construction deficiencies, the building with described details is named "as-designed" structure and is evaluated along with four variant structures that reflect the different construction faults mentioned in the previous section. These variant models are described in Table (1). Further details about the properties of these models were provided in the previous section.

The numerical models used for representing the above structures were developed in OpenSees finite element software [18]. Currently, two different methods are available for reflecting the plasticity of structural members; namely, distributed and concentrated (lumped) plasticity methods. The former includes the distribution of plasticity throughout the cross section and along the length of a frame member. The lumped plasticity method, on the other hand, assumes nonlinearity to concentrate in end regions of the members and reflects it in the moment-rotation behavior of some end springs. Each of these methods has abilities and limitations that should be considered before utilization in the modeling procedure.

The distributed plasticity method is featured with representing the gradual loss of stiffness during the loading process and the account for axial force-bending moment interaction. This method is not, however, capable to simulate plasticity sources other than the nonlinear stress-strain curves of the constitutive materials [19-20]. For RC members, these sources include:

a) The slippage of the reinforcements and their pull-out in the absence of adequate overlap or embedment length
b) The buckling of the compressive reinforcements due to inadequately-spaced transverse reinforcements or after considerable yielding of these bars; the crushing of the cover concrete can also accelerate the buckling of the longitudinal reinforcements

The lumped plasticity method, on the other hand, uses the moment-rotation curves observed in experimental tests performed on the members. This method is, therefore, capable to account for all the sources of plasticity occurring in the experiments including the above-mentioned sources. The disadvantage of this method is its neglect of axial force-bending moment interaction during the analysis of the member.

The distributed plasticity elements themselves use either force or displacement formulations. For a maximized accuracy, force-formulated distributed plasticity elements should be employed that follow the exact stability equations for deriving force interpolation functions used for distributing the end forces along the length of the element. However, the iterative procedure of this formulation encounters convergence problems in some models. To preclude this non-convergence, the RC beams and columns can be modeled using displacement-formulated elements. This formulation does not satisfy the force equilibrium but is featured with an enhanced efficiency which is gifted by the utilized displacement interpolation functions.

To evaluate the accuracy and efficiency of these methods for conducting the analyses required in this study, a sensitivity assessment is performed. For this purpose, the "as-designed" structure is modeled using the mentioned methods and is subjected to preliminary assessments. Regarding the results of this assessment, the appropriate method is selected and used for investigating the collapse performance of the structure in the presence of construction faults and mainshock-aftershock effects.

Table 1. Naming and description of the variant models used for reflecting design deficiencies.

Model Name	Description
As-designed	With the Designed Details
BeamWidth+	Employing Beams that are Aggregated with the Adjacent Joists
ColumnCover+	Employing Columns with Increased Concrete Cover
Story1Height+	Employing First Story Columns Longer than the Designed Height
ColumnStrength-	Employing Columns with Concrete Strengths Lower than the Design Value

4. Assessing alternative modeling methods and Validation

The two formulations of the distributed plasticity method as well as the concentrated plasticity method described in the previous section are deployed in this section for modeling the studied structure. These models are then subjected to sensitivity pushover and IDA analyses in order to evaluate their accuracies in a comparative manner.

To model the members through the distributed plasticity methods, the Concrete-01 uniaxial-material model of OpenSees is used for defining the fiber cross sections. This material model is a Kent-Scott-Park [21] stress-strain model with stiffness degra-dation and zero tensile strength [17]. Due to the non-convergence of the force-formulated model under dynamic excitations, this modeling method is excluded from this sensitivity assessment. For using the displacement formulation, each member should be divided into several segments to account for the neglect of the force stability in deriving the force-deformation relations of the element. The number of integration points can be limited to three in this case to eliminate unnecessary computation costs. For determining the optimum number of segments, an acceptable balance should be sought between the accuracy and the cost of the analyses.

The concentrated plasticity method, on the other hand, utilizes zero-length springs at the end parts of the frame elements. The moment-rotation behavior of these springs is defined using a peak-oriented version of the Ibarra-Medina-Krawinkler (IMK) model [22]. The zero-length elements correspond to a rotational hinge having a hysteretic response. The rotational hinge behavior is defined by uniaxial material models, which describe the moment-rotation or force-deformation relationship. The most recent OpenSees implementation, the peak oriented hysteretic model developed by Ibarra et al. [22] can be used to describe the behavior of the RC beam-column element. This model captures the four modes of cyclic deterioration, which includes the basic strength deterioration, the post-capping strength deterioration, the unloading stiffness deterioration, and the accelerated reloading stiffness deterioration. The model requires six parameters: elastic stiffness (K_e), effective yield strength (M_y),

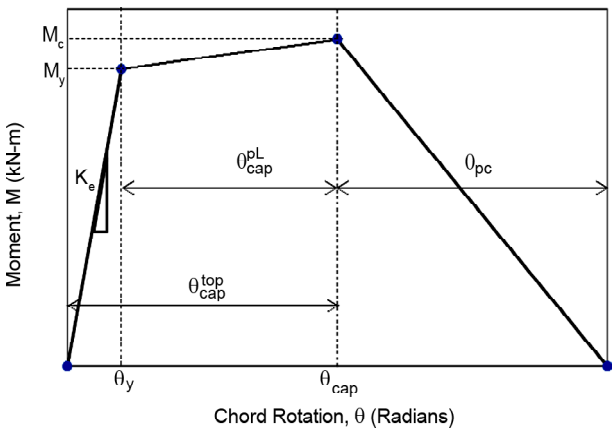

Figure 5. Monotonic behavior of component model developed by Ibarra et al. [22].

strain hardening ratio (M_c / M_y), pre-capping rotation (h_{cap}), post-capping rotation (*hpc*), and cyclic deterioration parameter (k). Figure (5) shows the moment-rotation law (backbone) according to Ibarra et al. [22].

The implementation of this model in OpenSees as the Clough uniaxial-material object [23] is utilized here. The flexural strength of the springs is computed by using the equivalent compressive stress block theory proposed by Panagiotakos and Fardis [24]. The cracked and post-yield stiffness values along with the ductility properties required for the definition of this model are computed through the empirical regression equations proposed by Mazzoni et al. [18]. To eliminate the convergence problems caused by a rigid-plastic flexural spring behavior, an equivalent series system is formed of the end springs and the internal elastic beam-column. Assuming a stiffness ratio of unity between the spring and the internal elements, the initial stiffness of these elements is modified so as to the overall stiffness of the series system equals the estimated cracked stiffness. This modification is also performed for the post-yield stiffness and the total energy absorption capacity of the springs used for determining the rate of cyclic deterioration in the IMK model.

A full-scale RC moment frame reported in Mohammad Noh et al. [25] was chosen for validation study. The selected RC Model is shown in Figure (6), and Sizes, reinforcement and mechanical properties of the frame are shown in Table (2). The loading program is based on displacement controlled loading cycles, with increasing displacements up to 30 mm. An axial compressive

load of 80 kN (14% of the column strength) was applied on the columns. Figure (7) shows cyclic loading obtained from both experimental and computational study. It can be seen that the computational is fairly matching with the experimental results.

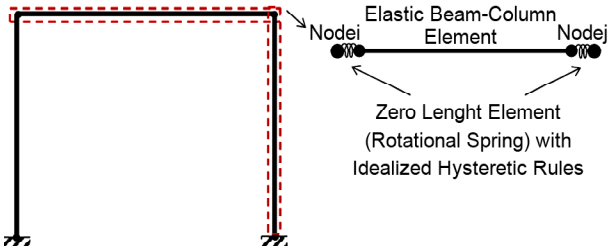

Figure 6. RC frame modeling using lumped plasticity elements [25].

Table 2. Geometric characteristic of RC frame in the experiment [25].

Design Characteristics	Experiment 2
Length (cm)-Axis to Axis of the Column	225
Height (cm)	172.5
Cross-Section of the Column (cm)	15 × 15
Cross-Section of the Beam (cm)	15 × 20
Longitudinal of Reinforcement of the Column	8Ø8
Tensile and Compression Reinforcement of the Beam	3Ø8
Stirrups	Ø4
Spacing Stirrups (cm)	7.5
Compressive Strength (MPa)	28.3
Yield Stress (MPa)	523
Ultimate Stress (MPa)	552

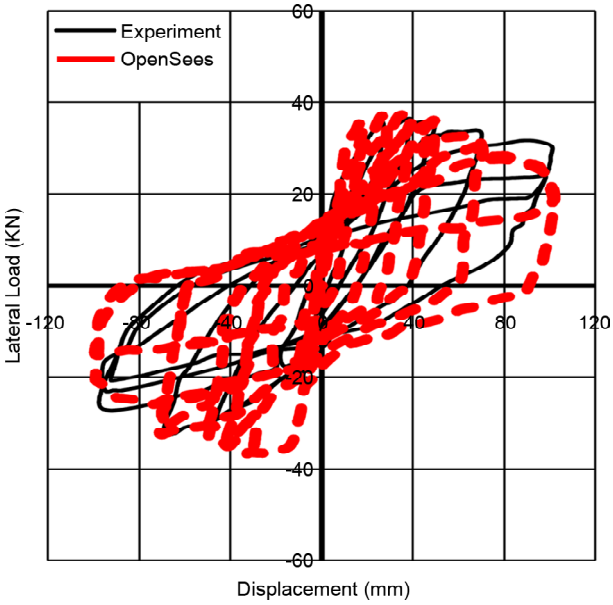

Figure 7. Experimental and computational responses of RC moment frame under cyclic loading [25].

As expressed before, the sensitivity of the analysis results to the alternative modeling methods is evaluated using static pushover and IDA results. While pushover may be adequate for investigating the monotonic load-displacement behavior predicted by the different methods, assessing cyclic effects such as the energy-based deterioration and the unloading-reloading behavior require a dynamic excitation. To see the variability in intensity and frequency content of the ground motion records, the dynamic analyses are performed using the IDA method. For this purpose, the 32 mainshock records introduced in the later sections of this study are utilized. Further details about these records and the IDA procedure are provided in section 5.

The pushover curves obtained by subjecting the displacement-formulated and the concentrated-plasticity "as-designed" models to a linear lateral load pattern are compared in Figure (8a). The distributed-plasticity results are denoted by a "Disp. N = n" naming convention where "Disp." denotes the utilization of displacement-formulated elements and n is the number of subdivisions of each element. As shown in Figure (8a), the accuracy of the pushover curves derived using displacement-formulated elements elevates by increasing the number of segments. However, the sensitivity of the curves to the subdivisions number reduces by increasing n. The pushover curve obtained using the described concentrated-plasticity method also leads to a medium accuracy that is comparable with the "Disp. N = 3" displacement-formulated model. The concentrated model shows around 30% difference, compared to the more accurate "Disp. N = 7" and "Disp. N = 10" curves under monotonic loading. Around 30% difference observed between these results, which is attributed to the more accurate account of the p-delta effects when the columns are subdivided through their length. The account of previously described damage modes by the concentrated-plasticity model leads to a steep descending branch after global drifts exceed the 0.03 value. This in-cycle degradation leads the concentrated-plasticity model to fall below the "Disp. N = 10" curve after an around 0.04 drift. This indicates that at large drifts, the more accurate account of damage modes by the concentrated-plasticity model compensates its lower accuracy in predicting

the p-delta effects. To decide about the acceptability of the different modeling methods, the cyclic performance of the models in different levels or response nonlinearity should also be addressed.

To assess the sensitivity of results to cyclic characteristics provided by various modeling methods, the median IDA curve derived using the N = 3 displacement-based model is compared against the curve obtained using the concentrated-plasticity model in Figure (8b). According to the Figure, the displacement-based model fails to simulate the softening of the model even when lateral drifts as large as 10% are reached. As a result, the median spectral acceleration, $S_a(T_1)$, corresponding to the collapse occurrence is estimated to be about 4.5 g using this model where g is the gravity acceleration. This is while the concentrated plasticity model shows a median collapse $S_a(T_1)$ of about 2.15 g. The significant difference between these results stems from the damage-caused in-cycle and cyclic degradations not accounted for in the distributed plasticity model. To further evaluate the predicted collapse capacities, they can be compared with the $S_a(T_1)$ of the maximum considered earthquake (MCE) prescribed by the design standard, which is 1.12 g for the studied building. According to the previous studies [26-27] on structures designed following common standards, the ratio between the median collapse $S_a(T_1)$ and the MCE $S_a(T_1)$ varies in a 2~3 range. Considering these findings reveals that the median collapse $S_a(T_1)$ predicted by the concentrated plasticity model is more realistic. Therefore, the concentrated plasticity method is utilized in the following parts of this study.

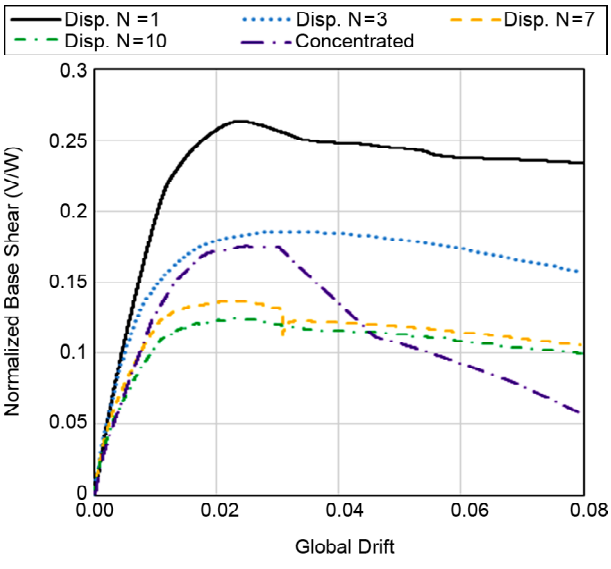

(a) Pushover Curves

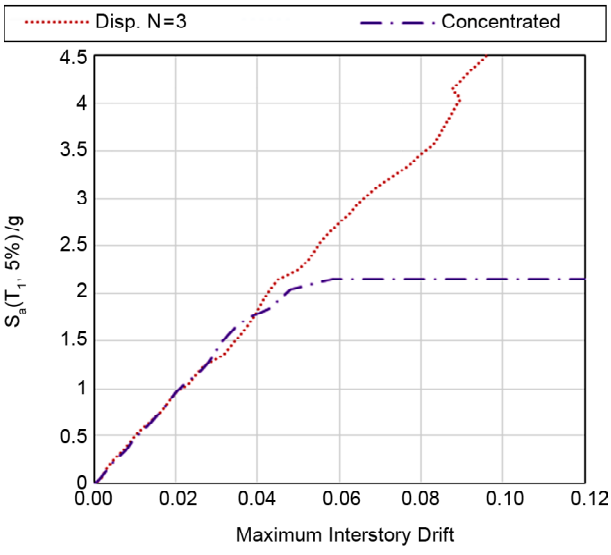

(b) Median IDA Curves Obtained Using the 32 Mainshock Records

Figure 8. Sensitivity of the "as-designed" model response to the selected modeling method.

5. Mainshock-Aftershock Collapse Assessment Methodology

As described in section 1, the collapse capacity of the studied structures is to be assessed by considering the mainshock-aftershock effects. To clarify the necessity of considering these effects, evidences of past earthquakes can be named in which aftershocks considerably contributed to the damage of structures. Some examples include the 1994 Northridge earthquake [28], the 1999 Chi-Chi earthquake [29], and the 2008 Wenchuan earthquake [30]. Regarding this significance, many studies have proposed methods for incorporating mainshock-aftershock effects. Studies by Mahin [31], Sunasaka & Kiremidjian [32] and Aschheim & Black [33] are among the first attempts that performed response history analyses on single degree of freedom (SDOF) systems. Studies on simplified SDOF systems continued till Lee & Foutch [34] who performed equivalent static loading on elastic degraded model of steel structures. The research by Luco et al. [12] is among the first studies performing complete response history analyses on multistory structures to assess the resistance of mainshock-damaged structures against the following aftershocks. By continual progression of the methods, Ryu et al. [35] implemented IDA [36] to capture the collapse capacity of structures in the presence of aftershock

excitations. Their method incorporated natural as-recorded mainshock-aftershock sequences and was later incorporated by other researchers including Li et al. [37] and Raghunandan et al. [38]. The latter also used repetition and randomization methods to represent mainshock-aftershock record sequences.

According to the above review on various mainshock-aftershock implementation methods, the method introduced by Lee and Foutch [34] is employed in this study. Within this method, the uncertainty of ground motion's frequency content is reflected by incorporating the IDA method. In performing IDA, each aftershock is increasingly scaled and applied to the structure until collapse of the structure is identified. To reflect the mainshock effect, it is imposed on the structure before each level of the aftershock and is followed by a free vibration analysis. The free vibration analysis allows complete damping of the shaking caused by the mainshock before the aftershock is applied. For mainshock-aftershock analyses, the IDA approach involves running NTHAs of the damaged structures, incrementally scaling up to the aftershock records with pre-recorded (scaled) mainshocks until the global collapse occurs.

By applying the IDA, the aftershock intensities corresponding to the structural collapse occurrence are recorded and presented statistically using a lognormal fragility curve. The variability of mainshock intensity is also accounted for by repeating IDAs and applying different scale factors to the mainshocks. To reduce the uncertainties associated with the mainshock intensity, scale factors are computed based on a target response parameter (e.g. maximum inter-story drift, MID) instead of intensity measures (IMs) commonly used in IDA.

According to ASCE-41 (ASCE 2006) [39], the structural performance for RC moment frames can be defined as three states. The performance states: immediate occupancy, life safety, and collapse prevention, are defined by 1.0%, 2.0%, and 4% transient drift, respectively. Also, in STD-2800, the amount of drift to ensure the performance of the structure subject to service earthquakes level is considered to be equal to 0.005. The three performance states can be viewed as minor, moderate, and severe damage for the RC frame. In addition, based on the IDA curves, the structural collapse capacity is determined as the last point on the IDA curve that is larger than the 20% of the initial tangent slope of the IDA [36]. This criterion is intended to consider the collapse. Regarding the implementation details, the mainshock scale factors are computed in correspondence with pre-selected MID values. These values are determined so that a wide range of mainshock damage levels is addressed. In this study, 0.0075, 0.02 and 0.04 values are selected as target MID values. Additionally, the mainshock is scaled to a level that poses the structure to the collapse threshold limit state. To scale each mainshock record to either of these response levels, the IM-MID curve of the record should be interpolated. This curve is obtained by an initial IDA of the building using mainshock records. As expressed above, after imposing the scaled mainshock, the structure should be allowed to freely vibrate for proper time duration. This duration depends on the record characteristics, the vibration magnitude and the damping content of the analyzed structure. To avoid selecting conservative duration times that are adequately large for all conditions, an interactive response-monitoring method is used in this article. This method and the required numerical tools were first employed by Jalali and Darvishan [40]. Using this method, the vibration amplitude is continually monitored during the free vibration analysis and the analysis is stopped after this amplitude becomes less than an acceptable tolerance.

Another implementation detail is related to the aftershock polarity. As a known fact, the maximum (positive) and minimum (negative) deformations induced by a record are not commonly of the same magnitude. Thus, changing the record direction by 180^{o} also affects the direction of the maximum response undergone by the structure. Although for symmetric structures this "polarity" does not alter the evaluation results, it should be addressed in presence of asymmetry. The residual deformations imposed by the mainshock pose some asymmetry to the building before an aftershock hits it. Therefore, the two possible polarities are checked and the one with the worst effects is imposed in this study.

In performing IDA using a mainshock-aftershock pair, the effect of mainshock should be imposed before applying each new scale of the aftershock.

This leads to the repetition of the mainshock and the free vibration analyses. To minimize the computational costs of performing mainshock-aftershock IDAs, this repetition is prevented here using the "database" command of OpenSees program. Using this command, the status of the model is saved at the first run just before the aftershock is imposed on the model. The next aftershock runs are then performed by setting the model status to the previously saved condition. This strategy led to around 50% saving in the time of mainshock-aftershock IDAs performed here.

For performing IDAs, 32 as-recorded mainshock-aftershock pairs previously used by Raghunandan et al. [38] are employed. The names and characteristics of these records is shown in Table (3).

Table 3. Mainshock-aftershock ground motions used in this study [38].

No.	Earthquake Name	Ms	Record Name	Station	Ref.
1	Coalinga	6.36	NGA_no_368_H-PVY045.AT2	Pleasant Valley P.P.–Yard	PEER
		5.09	NGA_no_383_A-PVY045.AT2		
2	Coalinga	6.36	NGA_no_368_H-PVY135.AT2	Pleasant Valley P.P.–Yard	PEER
		5.09	NGA_no_383_A-PVY135.AT2		
3	Chalfant Valley	6.19	ChalfantValley86_CE54171P.V2	Number 54171	CESMD
		5.44	ChalfantValley86C_CE54171P.V2		
4	Chalfant Valley	6.19	ChalfantValley86_CE54428P.V2	Number 54428	CESMD
		5.44	ChalfantValley86B_CE54428P.V2		
5	Chalfant Valley	6.19	ChalfantValley86_CE54424P.V2	Number 54424	CESMD
		5.44	ChalfantValley86B_CE54424P.V2		
6	Imperial Valley	6.53	NGA_no_162_H-CXO315.AT2	Calexico Fire STA	PEER
		5.01	NGA_no_195_A-CXO315.AT2		
7	Imperial Valley	6.53	NGA_no_174_H-E11140.AT2	El Centro Array 11	PEER
		5.01	NGA_no_199_A-E11140.AT2		
8	Imperial Valley	6.53	NGA_no_178_H-E03230.AT2	El Centro Array 3	PEER
		5.01	NGA_no_201_A-E03230.AT2		
9	Imperial Valley	6.53	NGA_no_172_H-E01230.AT2	El Centro Array 1	PEER
		5.01	NGA_no_197_A-E01230.AT2		
10	Imperial Valley	6.53	NGA_no_169_H-DLT262.AT2	Delta	PEER
		5.01	NGA_no_196_A-DLT262.AT2		
11	Livermore	5.8	Livermore80A_CE57187P.V2	Number 57187	CESMD
		5.42	Livermore80B_CE57187P.V2		
12	Livermore	5.8	Livermore80A_CE67070P.V2	Number 67070	CESMD
		5.42	Livermore80B_CE67070P.V2		
13	Livermore	5.8	NGA_no_212_A-DVD246.AT2	Del Valle Dam	PEER
		5.42	NGA_no_219_B-DVD246.AT2		
14	Livermore	5.8	NGA_no_214_A-KOD180.AT2	San Ramon Kodak Building	PEER
		5.42	NGA_no_223_B-KOD180.AT2		
15	Livermore	5.8	NGA_no_215_A-SRM070.AT2	San Ramon	PEER
		5.42	NGA_no_224_B-SRM070.AT2		
16	Livermore	5.8	NGA_no_213_A-FRE075.AT2	Fremont Mission S.J.	PEER
		5.42	NGA_no_220_B-FRE075.AT2		
17	Livermore	5.8	NGA_no_210_A-A3E236.AT2	Hayward CSUH Stadium	PEER
		5.42	NGA_no_217_B-A3E236.AT2		
18	Mammoth Lakes	6.06	NGA_no_231_I-LUL090.AT2	Long Valley Dam UPR L	PEER
		5.94	NGA_no_250_L-LUL090.AT2		
19	Mammoth Lakes	6.06	NGA_no_231_I-LUL090.AT2	Long Valley Dam UPR L	PEER
		5.7	NGA_no_243_B-LUL090.AT2		
20	Mammoth Lakes	6.06	NGA_no_231_I-LUL090.AT2	Long Valley Dam UPR L	PEER
		5.69	NGA_no_234_J-LUL090.AT2		
21	Northridge	6.69	NGA_no_963_ORR090.AT2	Castaic–Old Ridge Route	PEER
		5.93	NGA_no_1676_CASTA090.AT2		
22	Northridge	6.69	NGA_no_1039_MRP090.AT2	Moorpark	PEER
		5.93	NGA_no_1681_MPARK090.AT2		

Table 3. Continue.

No.	Earthquake Name	Ms	Record Name	Station	Ref.
23	Northridge	6.69	NGA_no_1005_TEM090.AT2	Los Angeles–Temple and Hope	PEER
		5.28	NGA_no_1712_TEMPL090.AT2		
24	Northridge	6.69	NGA_no_971_ELI180.AT2	Elizabeth Lake	PEER
		5.93	NGA_no_1677_ELIZL180.AT2		
25	Northridge	5.93	NGA_no_945_ANA180.AT2	Anaverde Valley–City Ranch	PEER
		6.69	NGA_no_1675_ANAVE180.AT2		
26	Northridge	6.69	NGA_no_990_LAC180.AT2	Los Angeles–City Terrace	PEER
		5.93	NGA_no_1678_CTYTE180.AT2		
27	Northridge	6.69	NGA_no_1007_UNI095.AT2	LA–Univ. Hospital GR	PEER
		5.93	NGA_no_1680_UNIHP090.AT2		
28	Petrolia	7.2	Petrolia_25Apr1992_CE89530P.V2	Number 89530	CESMD
		6.7	PetroliaAftershock2_26Apr1992_CE89530P.V2		
29	Petrolia	7.2	Petrolia_25Apr1992_CE89156P.V2	Number 89156	CESMD
		6.5	PetroliaAftershock1_26Apr1992_CE89156P.V2		
30	Petrolia	7.2	Petrolia_25Apr1992_CE89509P.V2	Number 89509	CESMD
		6.5	PetroliaAftershock1_26Apr1992_CE89509P.V2		
31	Whittier Narrows	5.99	NGA_no_615_A-DWN270.AT2	Downey	PEER
		5.27	NGA_no_709_B-DWN270.AT2		
32	Whittier Narrows	5.99	NGA_no_663_A-MTW000.AT2	Mt. Wilson	PEER
		5.27	NGA_no_715_B-MTW000.AT2		

The collapse of the buildings is identified following a dynamic instability criterion. For this purpose, the response of the structure is expressed using an engineering demand parameter (EDP) which appropriately represents the lateral performance of the structure. Using so, the slope of the IM-EDP curve can be regarded as an expression of the amount of strength and stiffness loss in the structure. Generally, the formation of plastic mechanisms and amplification of the second order moments in the presence of the lateral deformations are responsible for the behavior softening that eventually leads to the global instability and collapse. As suggested by performance-based guidelines such as FEMA P695 [26], EDP can be acceptably represented by the MID parameter in frame structures. Doing so, an 80% loss in the initial slope of the IM-EDP curve is suggested for identifying the collapse of the structure [27]. In conditions where global instability occurs in an MID > 0.1 value, the MID = 0.1 should be considered for rational estimation of the collapse capacity.

6. Results and Discussion

The medians of the IDA curves obtained using the described methodology are illustrated in Figure (9) for the different variant models and various mainshock damage levels. The first point to note about these curves is the shift-to-right and the reduction in the aftershock collapse intensity as the level of mainshock MID is increased. An exceptional observation is however made for the "ColumnStrength-" when the MID = 0.04 damage level is compared with the pre-collapse level. In this model, the aftershock collapse intensity is lower for the MID = 0.04 compared to the pre-collapse level. This observation reveals that the mainshock-induced collapse of the "ColumnStrength-" structure occurs at MID values less than 0.04.

Another important point to mention is the different shapes of the IDA curves obtained in the presence of mainshock damage levels corresponding to MID = 0.04 and the pre-collapse level. These curves start with an initial flat segment that change to the normal shape after reaching a certain level of MID value shown on the horizontal axis. This initial lag is the result of the residual story drifts caused by existing damages in the structures. Regarding this description, it can be said that the observed initial lag is a representative of the maximum residual drift (MRD) (maximum between the different stories) caused by the mainshock. To evaluate the MRD values imposed by the various mainshock levels to the different models, these values are plotted in Figure (10).

According to the figure plots, very slight residual drifts are caused by the MID = 0.0075 mainshock

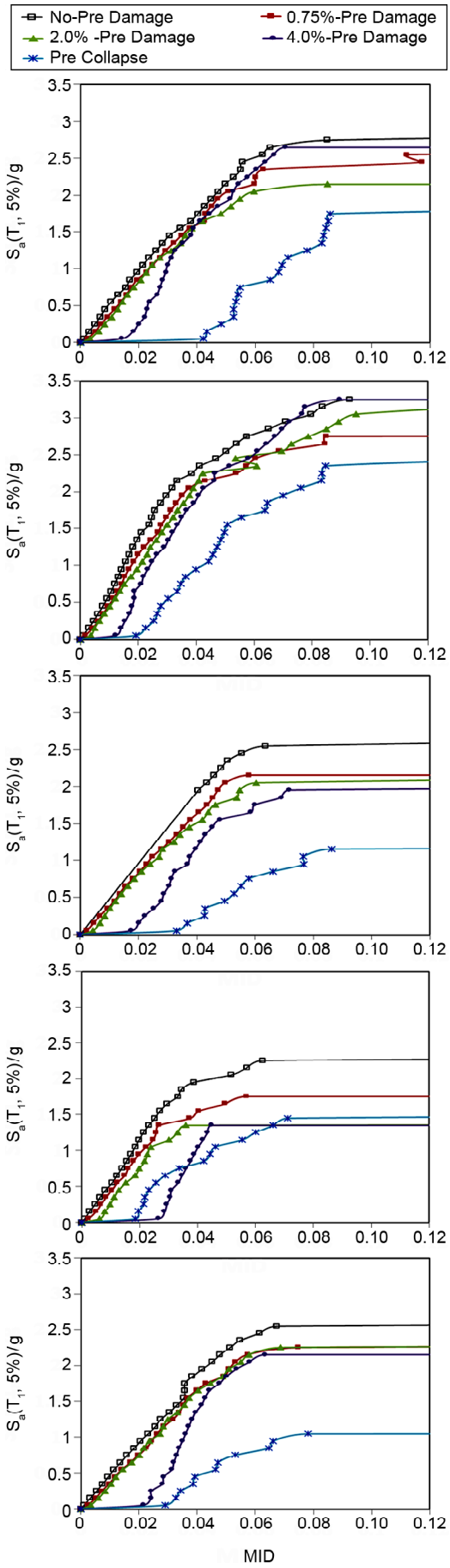

Figure 9. The median IDA curves of the variant models subjected to mainshock-aftershock IDAs with various mainshock MID levels.

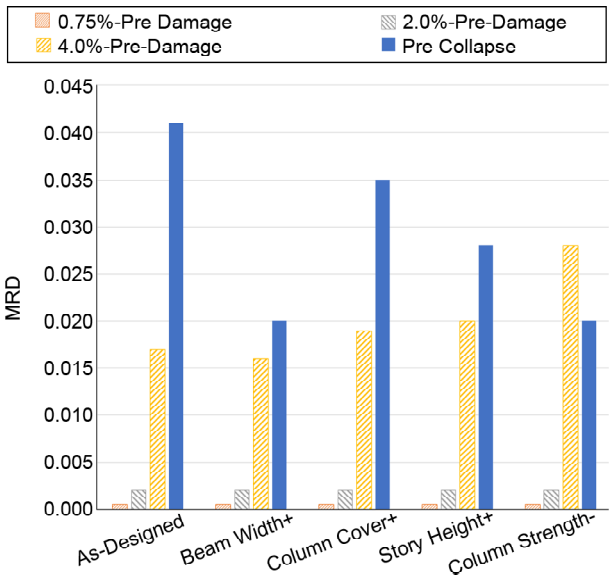

Figure 10. The MRD values observed at the end of various levels of mainshock excitations in the different models.

level in the different models. At the MID = 0.02 mainshock level, still MRDs less than 0.003 are observed by all the models. Considering the MID = 0.04 mainshock level, all construction faults except the BeamWidth+ case have undergone MRDs that are larger than the "as-designed" model. To interpret these observations, the magnitude of the MRDs undergone by the different structures after the MID = 0.04 mainshock excitation should be treated as the level of plasticity experienced during the mainshock. Accordingly, the comparison between the MRDs experienced by the different models at this mainshock level reveals the decreased plasticity level due to the "BeamWidth+" fault while all other deficiencies have caused the plastic response level to increase. The decreased plasticity of the "BeamWidth+" structure should be attributed to the enlarged stiffness and plastic capacity of the beams. This indicates that the increase of the beams' plastic capacity has not led to the violation of the SCWB principle. In the case of violating this principle, an increased plasticity of the structure would be expected due to the formation of plastic hinges in the columns and the resulting additional softening of the structure. It should be however noted that meeting the SCWB principle cannot prevent plasticity of the columns in all circumstances. That is, by increase of the lateral load or excitation level, the post-yield hardening stiffness of the beams will cause their force demands to continue growing. As a result, growth of the column forces

will also occur which may eventually lead to their yielding and formation of the column plastic hinges. The inelastic response levels experienced by the three "ColumnCover+", "Story1Height+" and "ColumnStrength-" deficient structures are respectively in the low, medium and large ranges.

Regarding the pre-collapse mainshock level, the MRD values should be interpreted as the level of plastic response the structures can tolerate before they undergo the lateral collapse. From this perspective, the "as-designed" structure shows the largest plastic deformation capacity while the "BeamWidth+" and "ColumnStrength-" structures collapse after the lowest levels of plasticity are undergone. As described above, at the collapse state caused by the mainshock, the larger capacities of the beams in the "BeamWidth+" structure, compared to the "as-designed" model, will increase the level of plasticity undergone by the columns. This is due to the decreased inelastic response and hysteretic energy dissipation provided by the beams in the "BeamWidth+" structure. As a result, larger energy absorption and response plasticity should occur in the columns to dissipate the seismic input energy. In the "ColumnStrength-" on the other hand, the reduced column strength has accelerated the formation of plastic hinges in the columns. It is therefore seen that both these models are characterized with an increased column plasticity. This infers that the most detrimental construction deficiencies, in terms of ductility content, are those that increase the columns plastic hinging and thereby cause a more fragile lateral load bearing mechanism. Considering the "ColumnCover+" deficient model, a reduced flexural strength is also expected to be provided by the columns. This reduction has not, however, led to the plasticity shifting observed in the two previously mentioned models. This observ-ation highlights the fact that a simultaneous reduction in axial and flexural strengths (as in the "ColumnStrength-" model) is more effective in accelerating the columns yielding than the sole reduction in the flexural capacity, which is the case for the "ColumnCover+" structure.

The 32 as-recorded seismic sequences are employed to investigate the effect of the damage states from mainshocks on the structural collapse capacity. Considering the aftershock Fragility Curves of Collapse Damage State shown in Figure (11), the

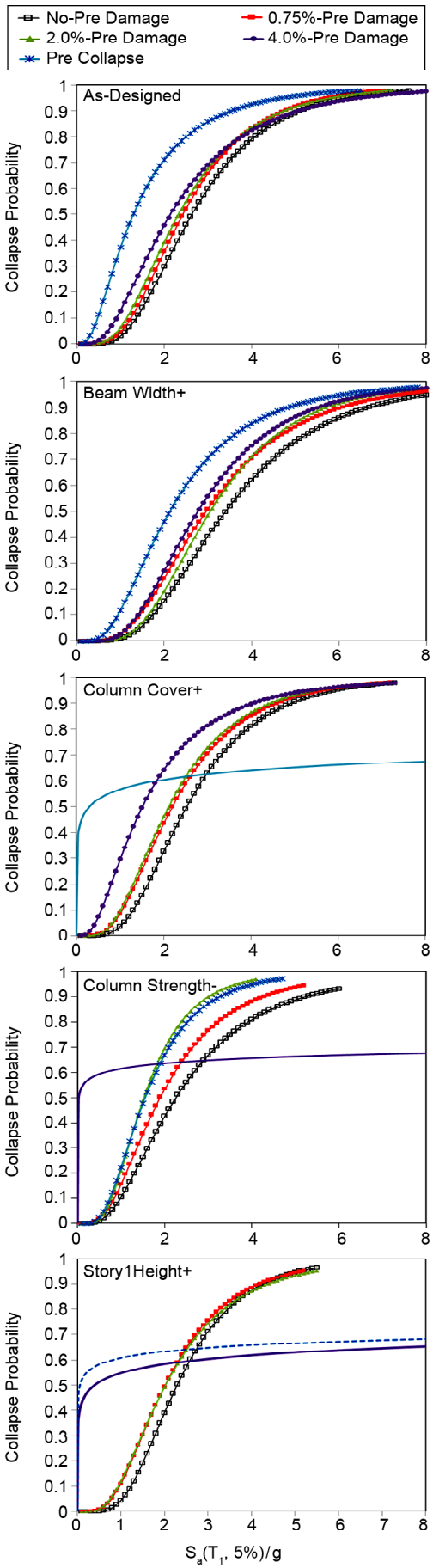

Figure 11. The collapse fragility curves of the variant models subjected to mainshock-aftershock IDAs with various mainshock MID levels.

increase in the mainshock damage level is seen to shift the curves to lower values with respect to the horizontal axis. This means the reduction in the $S_a(T_1)$ value corresponding to the 50% collapse probability. This $S_a(T_1)$ value is called median collapse capacity (MCC) and will be respected in the assessments performed in the following parts of this article. In some fragility curves, the very large dispersions of $S_a(T_1)$ values corresponding to the collapse state have caused the curve shape to differ remarkably from the others. These are typically the cases where the behavior degradation under mainshock damage has caused near-zero strength in the columns. Thus, the structure is hardly able to maintain its stability under the mainshock and the estimated collapse $S_a(T_1)$ values are subject to serious numerical instabilities.

The mean and standard deviation of the collapse damage state threshold for different structural performance states are listed in Table (4).

The MCC values corresponding to different mainshock damage levels and the variant structural models are compared in Figure (12a). Despite the previous finding that showed larger plastic demands of the "Beam Width+" structure at the collapse state, the capacity of this model expressed in terms of $S_a(T_1)$ is seen to surpass that of the "as-designed" model. To clarify these findings, it should be stated that the previous finding was related to a comparison between the collapse mechanisms of the two structures and showed the higher capacity of the "as-designed" structure in tolerating inelastic demands before the collapse state occurred. The MCC-related finding, however, reveals that the more ductile collapse mechanism of the "as-designed" structure is associated with lower collapse strength, expressed in $S_a(T_1)$ terms, compared to the "Beam Width+" structure. The rest of the deficient structures, namely "Column Strength-", "Column Cover+" and "Story1 Height+", show lower collapse capacities while they were also shown to possess reduced ductility contents.

Table 4. Statistics of Collapse Capacity.

Model Name	No-Pre Damage		0.75%-Pre Damage		2.0%-Pre Damage		4%-Pre Damage		Pre Collapse	
	μ	σ	μ	σ	μ	σ	μ	σ	μ	σ
As-Designed	2.91	2.49	2.72	2.48	2.76	2.48	2.91	2.49	2.5	2.47
Beam Width+	3.72	2.52	3.54	2.52	3.17	2.5	3.13	2.5	2.98	2.49
Column Cover+	2.8	2.48	2.76	2.48	2.65	2.48	2.8	2.48	3.41	2.57
Story1 Height+	2.13	2.44	2.02	2.43	2.13	2.44	3.54	2.65	3.05	2.64
Column Strength-	2.31	2.46	2.02	2.43	1.61	2.39	3.37	2.64	1.83	2.42

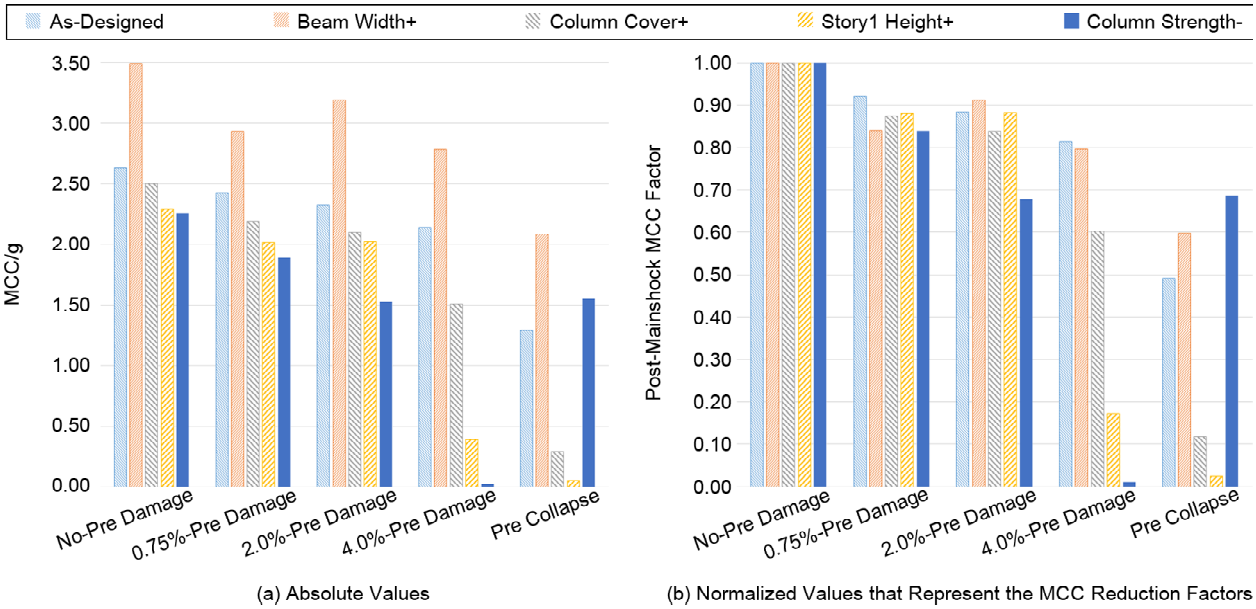

(a) Absolute Values

(b) Normalized Values that Represent the MCC Reduction Factors

Figure 12. The MCC values corresponding to different mainshock damage levels and the variant structural models.

To assess the effect of mainshock damage on the observed MCCs, the post-mainshock factor is computed by dividing the MCC values obtained in presence of various mainshock MID's by the no-pre-damage (aftershock-only) value. The computed post-mainshock MCC factors related to various mainshock damage levels and are depicted in Figure (12b). Comparing the bar charts related to the different models, rather similar factors are observed at the MID = 0.0075 mainshock level for the variant models.

By amplifying the mainshock damage to the MID = 0.02 level, the deficient model receiving the largest negative impact is seen to be the "Column Strength-" model. As was mentioned previously, this model experiences the highest column strength reduction among the different models with faulty column construction. This strength reduction has remarkably increased the susceptibility of this structure to the prior damage caused by the mainshock. As was stated before, this structure collapses before reaching the MID = 0.04 level. Thus, the aftershock MCC obtained at the MID = 0.04 mainshock level for this structure is actually the result of aftershock hitting an already collapsed structure and should not be considered as a meaningful data. The almost similar aftershock MCCs obtained for this structure at the two MID = 0.02 and pre-collapse mainshock levels, imply that the collapse of this structure occurs at MID values near 0.02. Said this, these results should be considered as different expressions of the same response.

Further intensification of the mainshock damage to MID = 0.04 level is associated with a dramatic drop in the post-mainshock MCC factor (= 17.5%) of the "Story1Height+" structure. The susceptibility of this model to the mainshock damage can therefore be ranked second after the "Column Strength-" structure. The reason for this susceptibility is the decreased ductility and plastic capacity of the columns at the first story of this structure. As was described in section 2.3, these columns suffer from inadequate transverse reinforcement in the lower end and also an unpredicted height increment. The first story is characterized, on the other hand, with the largest shear demand in a first-mode dominated excitation and the highest p-delta effects. These criticalities should be counted as the reason for the second vulnerability rank of this structure.

In the same MID = 0.04 damage level, the third vulnerability level there appears to belong to the "Column Cover+" structure with a 60% post-mainshock MCC factor. This factor drops to a 10% value at the pre-collapse mainshock level. As was stated before, this structure suffers from a moderate column strength reduction brought about by the lowered flexural capacity and maintained axial strength.

7. Conclusions

In this study, the mainshock-aftershock effects were considered in evaluating the collapse performance of low-rise RC moment frames suffering from construction faults. A field study was then performed to identify the most paramount construction deficiencies affecting collapse of the structures during the 2017 Sarpol-e Zahab earthquake in Iran. The available nonlinear modeling methods were next evaluated according to their capability to predict the collapse capacity of the studies structures. The lumped plasticity method was then selected for mathematical representation of the "as-designed" structure along with its four deficient variants. These variants included:

1) "Beam Width+" in which cast-in-place RC joists were adjoined to the beams during the construction and increased the beams width; this model reflected a common construction practice.
2) "Column Strength-" in which the concrete poured manually into the columns formworks had compressive strengths almost 45% lower than the design vale; a worst-scenario was used in defining this deficient model.
3) "Column Cover+" in which the bending capacity of the columns was lowered by doubling the concrete cover of the reinforcement bars; this model was also built following a worst-scenario method.
4) "Story1Height+" in which the height of the first story columns were increased by about 10% while the ductile details prescribed for the transverse reinforcements at the lower end of these columns were also omitted; this variant model reflected a common deficiency in the regional construction method.

Each of these models was the subjected to pre-selected damage levels by mainshock, followed by an IDA performed using aftershock. Doing so, the probabilistic collapse capacities of the structures under aftershock was extracted when varying MID levels were imposed by the mainshock. This procedure was carried out using 32 as-recorded mainshock-aftershock records and the maximum residual drifts (MRDs) caused by the mainshock were extracted along with median collapse capacities (MCCs) under the aftershocks.

Evaluating the median mainshock-induced MRDs at a level corresponding to the maximum story drift (MID) of 0.04 revealed the reduced plasticity undergone by the "BeamWidth+" structure compared to the "as-designed". At the pre-collapse mainshock level, however, the "as-designed" model experienced higher MRDs that showed the higher ductility capacity this structure could provide before a collapse event. Regarding the aftershock MCC parameter, larger values were possessed the "BeamWidth+" structure, compared to the "as-designed", denoting the higher strength level provided by this structure despite its reduced ductility. The vulnerability of this structure was therefore smaller than its "as-designed" counterpart.

With respect to the three other deficient structures, the ductility reductions were accompanied by strength drops that increased their vulnerability to the mainshock damage. Ranking the susceptibility of these structures by comparing their post-mainshock MCC factors, the "ColumnStrength-", "Story1Height+" and "ColumnCover+" structures were ranked from 1 to 3, respectively. A critical role was identified for the plastic hinges forming at the columns. The faulty construction methods were, thus, shown to suffer more when columns' plasticity remarkably preceded the beams'.

References

1. Imam, B. and Chryssanthopoulos, M. (2010) A review of metallic bridge failure statistics. Bridge Maintenance, Safety and Management: *Proceedings of the Fifth International IABMAS Conference*.
2. Hansson, E.F. (2011) Analysis of structural failures in timber structures: Typical causes for failure and failure modes. *Engineering Structures,* **33**(11), 2978-2982.
3. Melchers, R. (1989) Human error in structural design tasks. *Journal of Structural Engineering*, **115**(7), 1795-1807.
4. Ellingwood, B.R. (1994) Probability-based codified design: past accomplishments and future challenges. *Structural Safety*, **13**(3), 159-176.
5. Ellingwood, B.R. (2001) Acceptable risk bases for design of structures. *Progress in Structural Engineering and Materials*, **3**(2), 170-179.
6. Zhang, H., Rasmussen, K.J., and Ellingwood, B.R. (2012) Reliability assessment of steel scaffold shoring structures for concrete formwork. *Engineering Structures*, **36**, 81-89.
7. El-Shahhat, A.M., Rosowsky, D.V., and Chen, W.-F. (1993) Construction safety of multistory concrete buildings. *Structural Journal*, **90**(4), 335-341.
8. Epaarachchi, D.C., Stewart, M.G., and Rosowsky, D.V. (2002) Structural reliability of multistory buildings during construction. *Journal of Structural Engineering*, **128**(2), 205-213.
9. Epaarachchi, D.C. and Stewart, M.G. (2004) Human error and reliability of multistory reinforced-concrete building construction. *Journal of Performance of Constructed Facilities*, **18**(1), 12-20.
10. Hong, H. and He, W. (2015) Effect of human error on the reliability of roof panel under uplift wind pressure. *Structural Safety*, **52**, 54-65.
11. Gashti, E.H.N., Zarrini, M., Irannezhad, M., and Langroudi, J.R. (2014) Evaluation of traditional methods in construction and their effects on reinforced-concrete buildings behavior. *World Academy of Science, Engineering and Technology, International Journal of Civil, Environmental, Structural, Construction and Architectural Engineering*, **8**(12), 1275-1281.
12. Luco, N., Bazzurro, P., and Cornell, C.A. (2004) Dynamic versus static computation of the residual capacity of a mainshock-damaged building to withstand an aftershock. *13th World Conference on Earthquake Engineering*.

13. Yeo, G.L. and Cornell, C.A. (2005) *Stochastic Characterization and Decision Bases under Time-Dependent Aftershock Risk in Performance-Based Earthquake Engineering*. Pacifi Earthquake Engineering Research Center Berkeley, CA.

14. Li, Q. and Ellingwood, B.R. (2007) Performance evaluation and damage assessment of steel frame buildings under main shock-aftershock earthquake sequences. *Earthquake Engineering and Structural Dynamics*, **36**(3), 405-427.

15. IIEES (2017) *2017 Sarpol-e-Zahab Earthquake Report, Volume III, Structures and Lifeline*. International Institute of Earthquake Engineering and Seismology, Tehran, Iran.

16. Building and Housing Research Center (2013) *Standard No. 2800, Iranian Code of Practice for Seismic Resistant Design of Buildings*, 4th Edition.

17. ACI (2014) *Building Code Requirements for Structural Concrete, in ACI 318-14. 2014*. American Concrete Institute.

18. Mazzoni, S. et al. (2004) *OpenSees Users Manual*. PEER Center, University of California, Berkeley.

19. Haselton, C.B. (2008) *Beam-Column Element Model Calibrated for Predicting Flexural Response Leading to Global Collapse of RC Frame Buildings*. Pacific Earthquake Engineering Research Center.

20. Zareian, F., Lignos, D., and Krawinkler, H. (2010) Evaluation of seismic collapse performance of steel special moment resisting frames using FEMA P695 (ATC-63) methodology. *Proc. ASCE Structures Congress*, Orlando.

21. Park, R., Kent, D.C., and Sampson, R.A. (1972) Reinforced concrete members with cyclic loading. *Journal of the Structural Division*, **98**(st7).

22. Ibarra, L.F., Medina, R.A., and Krawinkler, H. (2005) Hysteretic models that incorporate strength and stiffness deterioration. *Earthquake Engineering and Structural Dynamics*, **34**(12), 1489-1511.

23. Altoontash, A. (2004) *Simulation and Damage Models for Performance Assessment of Reinforced Concrete Beam-Column Joints*. Stanford University Stanford, California.

24. Panagiotakos, T.B. and Fardis, M.N. (2001) Deformations of reinforced concrete members at yielding and ultimate. *Structural Journal*, **98**(2), 135-148.

25. Mohammad Noh, N., Liberatore, L., Mollaioli, F., and Tesfamariam, S. (2017) Modelling of masonry infilled RC frames subjected to cyclic loads: State of the art review and modelling with OpenSees. *Engineering Structures*, **150**, 599-621.

26. NIST, G. GCR 10-917-8 (2010) *Evaluation of the FEMA P-695 Methodology for Quantification of Building Seismic Performance Factors*. National Institute of Standards and Technology, Gaithersburg, MD.

27. FEMA P695 (2009) *Quantification of Building Seismic Performance Factors*. F.E.M. Agency, Editor. Washington, DC.

28. Hauksson, E., Jones, L.M., and Hutton, K. (1995) The 1994 Northridge earthquake sequence in California: Seismological and tectonic aspects. *Journal of Geophysical Research: Solid Earth*, **100**(B7), 12335-12355.

29. Kao, H. and Chen, W.-P. (2000) The Chi-Chi earthquake sequence: Active, out-of-sequence thrust faulting in Taiwan. *Science*, **288**(5475), 2346-2349.

30. Kawashima, K., Takahashi, Y., Ge, H., Wu, Zh., and Zhang, J. (2009) Reconnaissance report on damage of bridges in 2008 Wenchuan, China, earthquake. *Journal of Earthquake Engineering*, **13**(7), 965-996.

31. Mahin, S.A. (1980) Effects of duration and aftershocks on inelastic design earthquakes. *Proceedings of the 7th World Conference on Earthquake Engineering*.

32. Sunasaka, Y. and Kiremidjian, A.S. (1993) *A Method for Structural Safety Evaluation under Mainshock-Aftershock Earthquake Sequences*. John A. Blume Earthquake

Engineering Center.

33. Aschheim, M. and Black, E. (1999) Effects of prior earthquake damage on response of simple stiffness-degrading structures. *Earthquake Spectra*, **15**(1), 1-24.

34. Lee, K. and Foutch, D.A. (2004) Performance evaluation of damaged steel frame buildings subjected to seismic loads. *Journal of Structural Engineering*, **130**(4), 588-599.

35. Ryu, H., Luco, N., Uma, Sr., and Liel, A.B. (2011) Developing fragilities for mainshock-damaged structures through incremental dynamic analysis. *Ninth Pacific Conf. on Earthquake Engineering*, Auckland, New Zealand.

36. Vamvatsikos, D. and Cornell, C.A. (2002) Incremental dynamic analysis. *Earthquake Engineering and Structural Dynamics*, **31**(3), 491-514.

37. Li, Y., Song, R., and Van De Lindt, J.W. (2014) Collapse fragility of steel structures subjected to earthquake mainshock-aftershock sequences. *Journal of Structural Engineering*, **140**(12), 04014095.

38. Raghunandan, M., Liel, A.B., and Luco, N. (2015) Aftershock collapse vulnerability assessment of reinforced concrete frame structures. *Earthquake Engineering and Structural Dynamics*, **44**(3), 419-439.

39. ASCE-41 (2006) *Seismic Rehabilitation of Existing Buildings*. American Society of Civil Engineers, Reston, VA.

40. Jalali, S.A. and Darvishan, E. (2019) Seismic demand assessment of self-centering steel plate shear walls. *Journal of Constructional Steel Research*, **162**.